

Solar geoengineering may not prevent strong warming from direct effects of CO₂ on stratocumulus cloud cover

Tapio Schneider^{a,b,1}, Colleen M. Kaul^c, and Kyle G. Pressell^c

^aCalifornia Institute of Technology, Pasadena, CA 91125; ^bJet Propulsion Laboratory, California Institute of Technology, Pasadena, CA 91125; and ^cAtmospheric Sciences & Global Change Division, Pacific Northwest National Laboratory, Richland, WA 99354

Edited by Kerry A. Emanuel, Massachusetts Institute of Technology, Cambridge, MA, and approved October 7, 2020 (received for review February 27, 2020)

Discussions of countering global warming with solar geoengineering assume that warming owing to rising greenhouse-gas concentrations can be compensated by artificially reducing the amount of sunlight Earth absorbs. However, solar geoengineering may not be fail-safe to prevent global warming because CO₂ can directly affect cloud cover: It reduces cloud cover by modulating the longwave radiative cooling within the atmosphere. This effect is not mitigated by solar geoengineering. Here, we use idealized high-resolution simulations of clouds to show that, even under a sustained solar geoengineering scenario with initially only modest warming, subtropical stratocumulus clouds gradually thin and may eventually break up into scattered cumulus clouds, at concentrations exceeding 1,700 parts per million (ppm). Because stratocumulus clouds cover large swaths of subtropical oceans and cool Earth by reflecting incident sunlight, their loss would trigger strong (about 5 K) global warming. Thus, the results highlight that, at least in this extreme and idealized scenario, solar geoengineering may not suffice to counter greenhouse-gas-driven global warming.

global warming | geoengineering | cloud feedback

Solar geoengineering is predicated on the notion that the global effects of perturbations to the climate system principally depend on the net radiative-energy balance at the top of the atmosphere (TOA). Elevated greenhouse gas (GHG) concentrations make the atmosphere more opaque to thermal longwave radiation. Hence, immediately after a rise of GHG concentrations, the longwave radiative energy fluxes emanating from TOA weaken. The climate system responds by warming globally, until TOA balance between outgoing longwave and absorbed solar radiative energy fluxes is restored. Solar geoengineering attempts to short-circuit this process by artificially reducing the amount of solar radiation absorbed in the climate system, thus obviating the global-warming response of the climate system. Simulations with multiple climate models have shown that global warming owing to rising GHG concentrations indeed can be fully or partially compensated by reducing the amount of solar radiation that is being absorbed. This can be achieved, for example, by injecting scattering aerosols into the stratosphere (1–5). There usually are some regional disparities in the degree of compensation (6–8). Additionally, global-mean evaporation and precipitation weaken, even when greenhouse warming is compensated for by solar geoengineering. This occurs because the reduced solar radiative energy available to evaporate surface water is not completely compensated for by a weakened longwave radiative cooling of the surface, even when the TOA compensation of radiative fluxes is complete (9, 10). Of course, nonradiative effects of elevated GHG concentrations, such as ocean acidification and ecosystem effects, remain uncompensated for by solar geoengineering (3, 11, 12). Other risks of solar geoengineering include moral hazards and governance issues, particularly related to what is known as the termination shock—the rapid realization of warming avoided

up to that point if solar geoengineering were started and, at a later time, after more GHGs have accumulated, suddenly stopped (12–15).

But there is another set of risks of solar geoengineering that has not received the attention it deserves. It arises through direct effects of GHGs on clouds. It is well known that elevated GHG concentrations directly reduce or thin cloud cover because they modify the longwave radiative cooling within the atmosphere, even without any surface-temperature changes, but possibly amplified by them (16–20). Stratocumulus cloud decks over subtropical oceans, especially, are vulnerable to changes in longwave cooling: They are sustained by longwave cooling at their cloud tops, which drives turbulent air motions from the cloud tops downward and, thereby, couples stratocumulus decks to their moisture supply at the surface (21, 22) (Fig. 1). This longwave cooling weakens as GHGs, such as CO₂ and water vapor, accumulate in the atmosphere, in much the same way that the capacity of Earth's surface to cool itself radiatively is lower in humid nights than in dry. Weakening cloud-top radiative cooling, in turn, thins the clouds and reduces the amount of incident sunlight they reflect back to space (23–26). Because stratocumulus decks cover large swaths of tropical oceans, their albedo effect cools Earth globally. Subtropical marine stratocumulus clouds currently lower Earth's surface temperature by about 8 K in the global mean compared with what it would be if they were replaced by scattered cumulus clouds (27). Hence, elevated GHG concentrations may trigger substantial global warming by reducing the cooling effect stratocumulus clouds provide, even when all or much of the effect of GHGs at TOA is compensated by solar geoengineering.

Significance

Solar geoengineering that manipulates the amount of sunlight Earth absorbs is increasingly discussed as an option to counter global warming. However, we demonstrate that solar geoengineering is not a fail-safe option to prevent global warming because it does not mitigate risks to the climate system that arise from direct effects of greenhouse gases on cloud cover. High-resolution simulations of stratocumulus clouds show that clouds thin as greenhouse gases build up, even when warming is modest. In a scenario of solar geoengineering that is sustained for more than a century, this can eventually lead to breakup of the clouds, triggering strong (5°C), and possibly difficult to reverse, global warming, despite the solar geoengineering.

Author contributions: T.S. and C.M.K. designed research; T.S., C.M.K., and K.G.P. performed research; T.S., C.M.K., and K.G.P. analyzed data; and T.S. wrote the paper.

The authors declare no competing interest.

This article is a PNAS Direct Submission.

Published under the [PNAS license](#).

¹To whom correspondence may be addressed. Email: tapio@caltech.edu.

First published November 16, 2020.

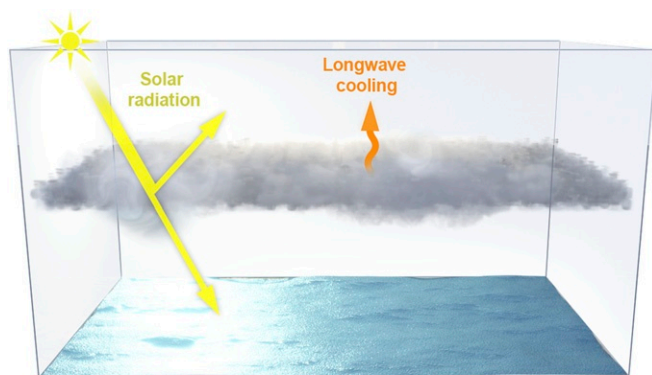


Fig. 1. Radiative energy fluxes at marine stratocumulus decks. Stratocumulus decks cool the surface by reflecting solar radiation. They are sustained by longwave radiative cooling of their cloud tops, which drives air motions downward and convectively connects the clouds to their moisture supply at the sea surface. When the concentration of GHGs, such as CO_2 and water vapor, increases, the longwave cooling of the cloud tops weakens, leading to cloud thinning and possibly, at high enough GHG concentrations, to breakup. Because these processes act through longwave radiation, they can lead to strong surface warming even under solar geoengineering scenarios.

We recently showed that stratocumulus decks may become unstable and break up at CO_2 concentrations above around 1,200 parts per million (ppm). This would trigger global warming of up to about 8 K, in addition to the warming that arose from the elevated CO_2 concentrations before the clouds broke up (27). Surface warming that led to enhanced evaporation and weakened cloud-top longwave cooling both played important roles in the stratocumulus instability. We obtained these results in a large-eddy simulation (LES) setup that inverts the standard approach in climate modeling: Instead of simulating the large-scale dynamics of the atmosphere explicitly in a general circulation model (GCM) while representing the important smaller-scale dynamics of clouds semiempirically, as is common, we simulated the dynamics of clouds explicitly and represented large-scale dynamics semiempirically. This approach complements GCM studies by focusing computational effort not on large-scale dynamics, as in GCMs, but on clouds—one of the principal uncertainties in the global climate response to elevated GHG concentrations. Here, we used the same simulation setup to investigate how stratocumulus decks respond to elevated GHG concentrations in an idealized solar geoengineering scenario.

Simulation Setup

As have many previous LES studies (23, 25, 28), we explicitly simulate the dynamics of the atmosphere over a patch of subtropical ocean (a $4.8 \times 4.8 \text{ km}^2$ area). The conditions in the patch are typical of summertime in areas that currently have persistent stratocumulus cover, such as off the coasts of California, Peru/Chile, or Namibia. We take the subtropical LES domain to be representative of 6.5% of the area of the globe—roughly the fraction of the globe currently covered by subtropical marine stratocumulus clouds (27). The subtropical LES domain is coupled 1) to the underlying sea-surface temperature (SST) through radiative and other energy fluxes (26, 29), and 2) to simple, but physically plausible, representations of large-scale atmosphere motions, including energy and water transports and a column model of the tropical atmosphere (27, 30). As shown in our previous study (27), a baseline simulation with 400 ppm CO_2 (approximately today's level) reproduces subtropical stratocumulus decks similar to those observed, with realistic underlying SSTs of 290 K in the subtropics and 300 K in the tropics.

Taking this baseline simulation as the point of departure, we increased CO_2 concentrations while reducing TOA insolation

uniformly by $3.7 \text{ W} \cdot \text{m}^{-2}$ for every CO_2 doubling. The magnitude of the insolation reduction is comparable to the global-mean longwave radiative forcing of CO_2 at TOA in climate models (16, 31, 32); in our modeling setup, it compensates about 70% of the longwave radiative forcing of CO_2 (*Materials and Methods*). Thus, a portion of the longwave radiative effect of CO_2 at TOA remains uncompensated, as in other solar geoengineering studies (e.g., refs. 1 and 8). The insolation reduction crudely mimics solar geoengineering, for example, by stratospheric aerosol injection (3, 10); we refer to these simulations as solar geoengineering simulations.

We performed three sets of solar geoengineering simulations: one in which the large-scale subsidence above the clouds in the subtropics was kept fixed; one in which the large-scale subsidence weakened moderately with warming (by 1% for each 1 K tropical surface warming); and one in which the large-scale subsidence weakened more strongly (by $3\% \text{ K}^{-1}$). The simulations with weakened subsidence were motivated by the fact that tropical circulations generally weaken under warming, primarily because weakened vertical mass fluxes are required to balance differential changes in precipitation and in atmospheric moisture content (or moisture stratification) under warming (33–36). Additionally, tropical circulations weaken because radiative effects of increasing GHG concentrations vary with latitude; however, this direct GHG effect is weak and of inconsistent sign in subtropical stratocumulus regions (37). Because it is unclear how much subsidence in subtropical stratocumulus regions (as opposed to in the tropical mean) weakens when both GHG concentrations increase and insolation is reduced, we explored the scenarios of no, $1\% \text{ K}^{-1}$, and $3\% \text{ K}^{-1}$ subsidence weakening as illustrative cases. We hope these span what may happen in reality or in more comprehensive models, which will eventually be needed to refine or refute our results (*Materials and Methods*).

Results

Simulation Results with Fixed Subsidence. In the simulations with fixed subsidence, when we doubled CO_2 concentrations from 400 to 800 ppm while reducing insolation, cloud cover in the subtropics remained at 100%, subtropical SST rose 1.2 K, and tropical SST rose 1.5 K (Fig. 2 A, D, and E). This is roughly half the SST increase in the corresponding simulations without solar geoengineering, in which subtropical SST rose 2.2 K and tropical SST rose 3.6 K (27). Surface temperatures still increased, although the insolation was reduced in the solar geoengineering simulations, in part because some of the radiative forcing of CO_2 was uncompensated by our solar geoengineering, and in part because the stratocumulus decks thinned (Fig. 2B). The stratocumulus thinning in the solar geoengineering simulations was, to within sampling variability, the same as in the simulations without solar geoengineering (27): In either case, liquid water path (LWP) in the clouds decreased by about $2.5 \mu\text{m}$ per doubling of CO_2 concentrations. This indicates that it is primarily the direct CO_2 effect that is responsible for the cloud thinning, rather than the surface warming. The stratocumulus thinning reduced the shortwave cloud radiative effect (CRE; Fig. 2C)—the reflection of sunlight by the clouds weakened. As a result, the absorption of sunlight in the subtropics strengthened, leading to surface warming, which is moderated by energy transport that, in our model, spreads excess energy accumulating in the subtropics homogeneously across the globe. The excess solar energy absorbed in the subtropics as a result of cloud thinning ($7.8 \text{ W} \cdot \text{m}^{-2}$; Fig. 2C) was about an order of magnitude larger than the uncompensated CO_2 radiative forcing at TOA (about $0.8 \text{ W} \cdot \text{m}^{-2}$).

The same general tendencies of moderate SST increases, thinning clouds, and reduced shortwave CRE, but with cloud coverage remaining at 100%, continued up to CO_2 concentrations of

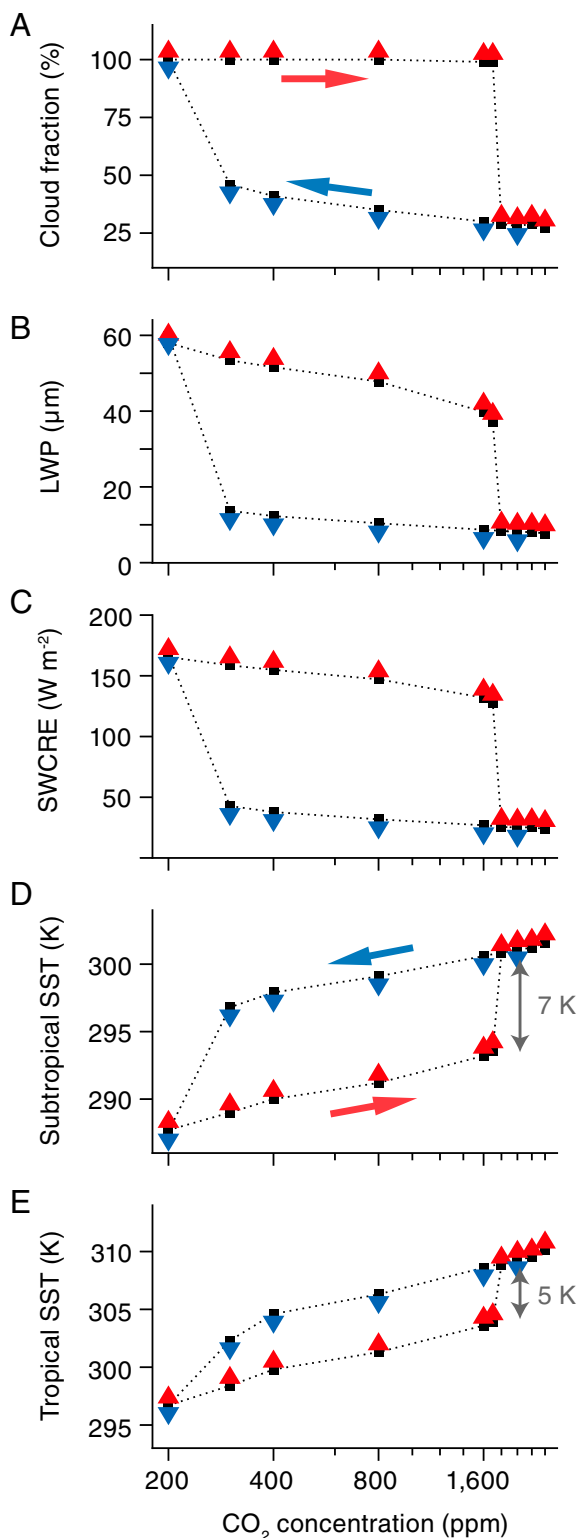


Fig. 2. Stratocumulus breakup and hysteresis under solar geoengineering with fixed subsidence. (A) Subtropical cloud fraction. (B) Cloud LWP. (C) Shortwave CRE (SWCRE) at TOA. (D) Subtropical SST. (E) Tropical SST. Red upward arrows indicate solar geoengineering simulations started from the baseline simulation with 400 ppm CO₂; blue downward arrows indicate simulations started from 2,400 ppm. The CO₂ axis is logarithmic (ticks every 200 ppm) because the radiative forcing of CO₂ is approximately logarithmic in concentration. TOA insolation is reduced by 3.7 W·m⁻² for every CO₂ doubling above 400 ppm to mimic solar geoengineering; TOA insolation is fixed for simulations with 400 ppm CO₂ or lower.

1,700 ppm. When CO₂ concentrations were increased further to 1,800 ppm, the stratocumulus decks became unstable and broke up into scattered cumulus clouds, as in the simulations without solar geoengineering (27). Cloud coverage collapsed from 100% to 30%, and shortwave CRE dropped from 155 W·m⁻² (400 ppm) to 26 W·m⁻² (1,800 ppm), triggering an abrupt subtropical SST increase of 7 K and a tropical SST increase of 5 K (Fig. 2). These temperature jumps were slightly smaller than in the simulations without geoengineering (27) because they occurred at reduced insolation, when the temperature effect of the albedo drop associated with cloud breakup was weaker. As in the simulations without geoengineering, the tropical SST increase can be taken as a proxy of the induced global warming because the excess energy accumulating in the subtropics is assumed to be spread homogeneously into the tropics and into other areas of the globe.

The simulations exhibit bistability as a function of CO₂ concentration, which leads to hysteresis (27). When CO₂ concentrations were lowered again after stratocumulus decks had broken up, the stratocumulus decks only reformed once CO₂ concentrations dropped below 300 ppm (Fig. 2 A–C)—a level below present-day concentrations. Until the stratocumulus decks reform, the climate in our model remains on a warm branch: The subtropical SSTs lie about 8 K and tropical SSTs about 5 K above the simulations in the colder branch, which have stratocumulus decks at the same CO₂ concentrations (Fig. 2 D and E).

Instability and Bistability Mechanism. A minimal conceptual model (21) suggests that stratocumulus decks decouple from their moisture supply at the surface and break up when the instability parameter $S = (\text{LHF}/\Delta L) \times (h_c/h)$ exceeds a critical $O(1)$ value. Here, ΔL is the longwave cooling of the cloud tops, LHF is the latent heat flux at the surface, h_c is the geometric thickness of the cloud, and h is the cloud-top height (27). The critical value of the instability parameter S lies approximately between 0.6 and around 1 (depending on the efficiency with which turbulence entrains dry and warm air from the free troposphere into the cloud).

In our simulations, the instability parameter S gradually increased from 0.4 at 400 ppm to 0.7 at 1,700 ppm, before the breakup at 1,800 ppm (Fig. 3D). The primary contributor to the increase in S is the weakening longwave cooling ΔL : It weakened by 22% as CO₂ concentrations rose from 400 to 1,700 ppm (Fig. 3A). The cloud-top cooling weakened because the longwave opacity of the atmosphere increases with increasing CO₂ concentrations. Increasing water-vapor concentrations owing to the moderate warming in the simulations also contributed to the opacity increase. The water-vapor feedback in the simulations without geoengineering is responsible for about 50% of the change in longwave cooling, as determined by offline radiative transfer calculations (27). Given that the warming in the solar geoengineering simulations was about a factor of 2 weaker, we estimate the water-vapor contribution to the change in longwave cooling to be about 25% in the solar geoengineering simulations. Strengthening evaporation (LHF), associated with surface warming, also contributed to the increase in S . Its contribution is smaller than the changes in longwave cooling: LHF strengthened by 17% from 400 to 1,700 ppm (Fig. 3B). The fraction h_c/h of boundary-layer thickness occupied by cloud did not change substantially because geometric cloud thickness h_c and the boundary-layer height h decreased roughly in unison (Fig. 3C). Thus, what sets off the instability of the stratocumulus decks is primarily the weakening longwave cooling of the cloud tops, augmented by evaporation enhancement. Eventually, the turbulent air motions that sustain the clouds decoupled from the moisture supply at the surface, leading to breakup.

At the breakup, longwave cooling dropped by a factor of 10 (with the factor of 3 drop in cloud fraction contributing a part),

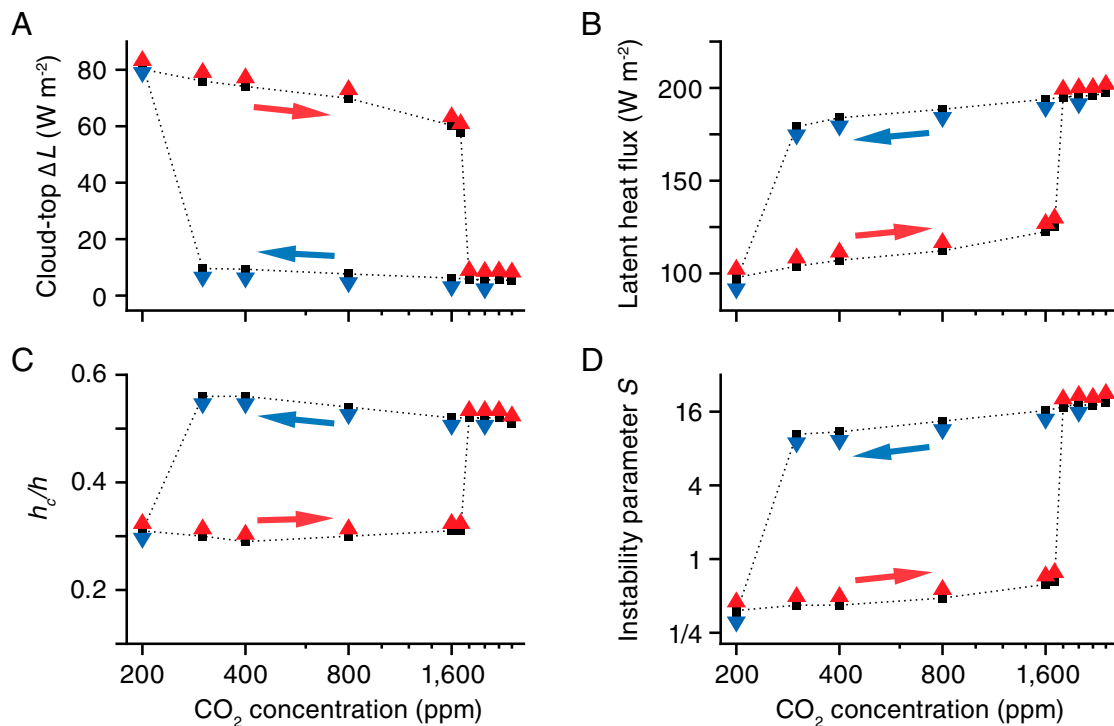


Fig. 3. Factors controlling stratocumulus stability under solar geoengineering with fixed large-scale subsidence. (A) Longwave radiative cooling of cloud tops (ΔL). (B) LHF at the surface. (C) Fraction of boundary-layer thickness occupied by cloud (h_c/h). (D) Instability parameter $S = (\text{LHF}/\Delta L) \times (h_c/h)$, on a logarithmic axis. (Plotting conventions are as in Fig. 2, and analysis methodology is as in ref. 27.)

and evaporation jumped by a factor of 1.6 (Fig. 3). The central nonlinearity responsible for the large changes in longwave cooling and evaporation and, ultimately, for the bistability and hysteresis is the interaction with the surface that accompanies the breakup. The large changes in longwave cooling and evaporation arise because when the reflection of solar radiation by the clouds weakens, the surface warms, and the atmosphere moistens (36). The added water vapor is in itself a GHG, suppressing longwave cooling and preventing the stratocumulus decks from reforming immediately when CO_2 concentrations are lowered again. Additionally, the enhanced evaporation in a warmer climate amplifies these processes because it, in itself, increases S and suppresses stratocumulus clouds (21). The role of water vapor in the instability also explains why the breakup of the stratocumulus decks occurs at higher CO_2 concentrations in the simulations with solar geoengineering than in those without: Water-vapor feedback roughly doubles the effect of CO_2 on the cloud-top longwave cooling in the simulations without solar geoengineering (27); it and evaporation enhancement are both reduced in the solar geoengineering simulations, in which surface warming is dampened.

The same mechanisms that are responsible for the stratocumulus breakup are also involved in the stratocumulus–cumulus transition in the present climate. The stratocumulus–cumulus transition occurs as trade winds advect air masses from eastern subtropical ocean basins westward and equatorward (21, 22, 38). The transition often occurs quite rapidly, over 1 to 3 d (39). Increasing surface temperatures and strengthening evaporation are thought to be primarily responsible for the stratocumulus thinning along the stratocumulus–cumulus transition in the present climate (40). This contrasts with the stratocumulus–cumulus transition in our solar geoengineering simulations, in which weakening cloud-top cooling plays a central role. Nonetheless, the surface warming that is essential for the stratocumulus–cumulus transition in the present climate is

also crucial for the transition in our solar geoengineering simulations: The feedback between cloud thinning and surface warming is what accounts for the abruptness of the transition and the bistability in our simulations. The stratocumulus–cumulus transition in the present climate is additionally associated with a weakening of the inversion near the cloud tops (40, 41). In our solar geoengineering simulations, by contrast, the inversion strength remained essentially unchanged as CO_2 concentrations increased. In the simulations without solar geoengineering, the inversion strengthened as CO_2 concentrations increased, consistent with the stronger surface warming and enhanced warming of the free troposphere, whose thermal stratification is moist-adiabatic. Thus, changes in inversion strength are not responsible for the stratocumulus breakup in the climate-change simulations with or without geoengineering (26).

Simulation Results with Weakened Subsidence. The solar geoengineering simulations in which subsidence weakened moderately ($1\% \text{ K}^{-1}$) were qualitatively similar to the simulations with fixed subsidence (Fig. 4 A–E). The main difference was that the breakup of the stratocumulus decks occurred at higher CO_2 concentrations, above 2,000 ppm. The bistability and hysteresis remained, with stratocumulus decks reforming once CO_2 concentrations dropped below 800 ppm. By contrast, in the simulations with stronger subsidence weakening ($3\% \text{ K}^{-1}$), the clouds still gradually thinned as CO_2 concentrations rose (Fig. 4 F–J). But within the range of CO_2 concentrations we simulated (up to 4,000 ppm), no stratocumulus instability occurred, and the stratocumulus decks remained intact, with nearly 100% cloud cover (Fig. 4F). The subsidence weakening counteracted the substantial cloud thinning and weakening shortwave CRE (Fig. 4 G and H) just enough to prevent a cloud breakup. However, given that the gradual cloud thinning and weakening shortwave CRE still occur, breakup may eventually happen at yet higher CO_2 concentrations.

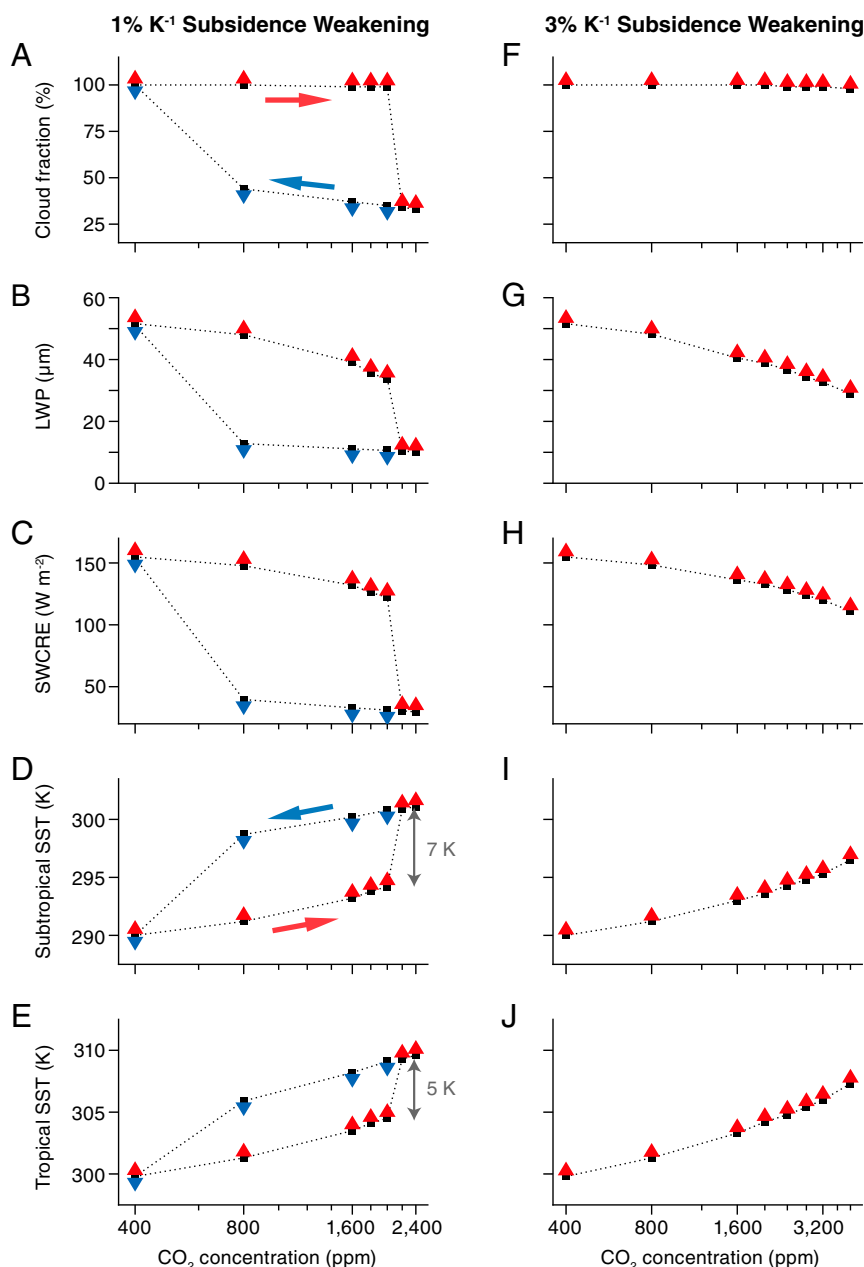


Fig. 4. Clouds and surface temperatures with weakening subsidence. (A and F) Subtropical cloud fraction. (B and G) Cloud LWP. (C and H) Shortwave CRE (SWCRE) at TOA. (D and I) Subtropical SST. (E and J) Tropical SST. (Left) Solar geoengineering simulations with subsidence weakening of $1\% \text{ K}^{-1}$ tropical SST increase. (Right) Simulations with subsidence weakening of $3\% \text{ K}^{-1}$. Red upward arrows indicate simulations started from 400 ppm CO_2 ; blue downward arrows indicate simulations started from 2,400 ppm. As in Fig. 2, the CO_2 axis is logarithmic, with ticks every 200 ppm in Left and every 400 ppm in Right.

Discussion

Our results show that solar geoengineering may not be a fail-safe option to counter global warming. At least in extreme and idealized solar geoengineering scenarios, rising GHG concentrations can eventually lead to breakup of subtropical stratocumulus decks. Because our model assumes that the extra solar energy absorbed when subtropical stratocumulus decks break up is spread uniformly across the globe, the tropical SST increase of around 5 K can be taken as a proxy for the global warming triggered by stratocumulus breakup. That is, even with solar geoengineering, strong global warming can occur if CO_2 continues to accumulate in the atmosphere to reach concentrations more than four times today's. It would take over a century to reach such CO_2 concentrations, even if emissions increase further (42).

Extending solar geoengineering to such high CO_2 concentrations is not currently considered. And it is possible that the stratocumulus breakup and attendant warming can be delayed to yet higher CO_2 concentrations if solar radiation is managed even more aggressively, so that there is no surface temperature increase initially. If stratocumulus breakup eventually occurs, the warming it triggers dramatically amplifies the termination shock that would occur if solar geoengineering were stopped thereafter.

Several caveats are in order. The thinning of stratocumulus clouds under increasing CO_2 concentrations is robust and well established (24). The amplifying feedback between thinning clouds and a warming sea surface is likewise rooted in well-understood physics, and that it can run away and lead to

stratocumulus breakup is physically plausible. The mechanisms involved are known to play a role in the stratocumulus–cumulus transition in the present climate (21). However, it remains unclear at which CO₂ concentrations breakup of stratocumulus may occur. Our simulations with different subsidence rates illustrate some of the difficulties of quantifying the critical CO₂ concentrations for stratocumulus breakup. But because our modeling setup lacks explicit representation of spatial heterogeneity and of temporal variations, such as the seasonal cycle and large-scale weather variability (meteorological noise), the real uncertainties are even greater. Spatial heterogeneity means that stratocumulus breakup, if it occurs in reality, would occur first in regions and seasons in which the stratocumulus decks are close to the stability threshold, likely at the margins of current stratocumulus regions (27). The lack of spatial heterogeneity and temporal variability in our simulations make it difficult to quantify more precisely the range of CO₂ concentrations over which stratocumulus breakup may occur, or when the clouds reform after CO₂ concentrations are lowered. The sources of noise neglected in our simulation may also reduce the width of the hysteresis loop and render the transitions between the states with and without stratocumulus decks less sharp as a function of CO₂ concentration than they are in our simulations (27). These are some of the limitations that come with the idealizations that were necessary to clearly illustrate the mechanisms involved and make this study computationally feasible; we plan to overcome these limitations in future work. Furthermore, we have not addressed the question of which, if any, solar geoengineering method may provide sufficient reductions in absorbed solar radiation to offset the radiative forcing of quadrupled (or higher) CO₂ concentrations; it is unclear whether such extensive solar geoengineering would be feasible (12, 14).

Caveats and limitations notwithstanding, the results illustrate a hitherto-unrecognized risk of solar geoengineering. It stems from the effects of elevated CO₂ concentrations on cloud cover, which generally reduce or thin cloud cover and are amplified by the surface warming that results from reduced or thinned cloud cover (16–20). These effects are difficult to offset by manipulating the amount of solar radiation Earth absorbs. The idealizations of our study bring limitations with them, especially with regard to quantitative statements about the CO₂ concentrations at which stratocumulus breakup occurs. Nonetheless, the results highlight that the relative risks and benefits of solar geoengineering remain insufficiently understood and quantified. It is imperative to understand and quantify these risks and benefits better. Doing so will require developing climate models that capture clouds, and especially low clouds, more accurately than do current models (43).

Materials and Methods

Experimental Design. The experimental design follows our previous study (27), which, in turn, builds on refs. 26 and 29. We performed the numerical experiments with the Python Cloud Large Eddy Simulation (PyCLES) code (44), employing an implicit LES approach with nominally fifth-order weighted essentially nonoscillatory advection schemes (45). The LES domain extends 4.8×4.8 km in the horizontal and 2.25 km in the vertical, with a horizontal grid spacing of 50 m and a vertical grid spacing of 10 m. The lower boundary of the subtropical LES domain is a thermodynamic slab ocean whose surface temperature evolves according to the surface-energy balance. The LES domain is coupled to a tropical column that is taken to be in radiative-convective equilibrium (RCE), with a moist-adiabatic temperature stratification and with an energetic imbalance at TOA that implies energy export out of the tropics. The horizontal temperature gradients between the tropical and subtropical free troposphere are assumed to be weak, and the free-tropospheric temperature profile in the subtropical LES domain is relaxed toward that of the tropical column (30, 46). In turn, the tropical column is coupled to the subtropical LES domain through energy transport: Any excess energy accumulating in the LES domain (beyond that implied by the TOA radiative energy flux imbalance in the baseline simulation with 400 ppm) is assumed to be spread homogeneously across

the globe, warming the tropical column as well as the rest of the globe. The resulting warming depends on the area fraction γ of the globe that the subtropical LES domain is assumed to represent. We take this to be $\gamma = 6.5\%$, based on the observation that subtropical marine stratocumulus cover 18.5% of the oceans between 5° and 35° latitude in both hemispheres, and this subtropical ocean area makes up 35% of Earth's surface area (47), so $\gamma = 0.185 \times 0.35 = 6.5\%$. Radiative energy fluxes are calculated with the Rapid Radiative Transfer Model for GCMs (48). Other details of the experimental setup, including how the tropical RCE state was calculated and how microphysical processes were represented, are described in ref. 27. The only difference to our previous study is the specification of TOA insolation.

Insolation. As in our previous study (27), the downwelling solar radiative-energy fluxes in the baseline simulation are $471 \text{ W}\cdot\text{m}^{-2}$ in the subtropical LES domain and $356 \text{ W}\cdot\text{m}^{-2}$ in the tropical column. These fluxes correspond to diurnally averaged insolation in July at 30°N and at the equator, respectively, where the equatorial insolation in July has been reduced by a factor $(1 - \alpha_t)$ ($\alpha_t = 0.09$) to account for the effective albedo of tropical clouds. Not explicitly simulating a diurnal cycle, we used a diurnally averaged solar zenith angle, which leads to biases in the diurnally averaged reflected solar radiation (49). These biases are of similar magnitude as biases from neglect of three-dimensional radiative transfer effects (50), with the latter partially compensating the former in our results. The simplifications in the representation of radiative transfer are among the several idealizations of this study that may affect quantitative details of the results.

Solar geoengineering is represented in an idealized fashion through modification of the TOA insolation relative to the baseline simulation. To offset the direct radiative forcing of increased CO₂ concentrations, TOA insolation was reduced by $3.7 \text{ W}\cdot\text{m}^{-2}$ per doubling of CO₂ concentration relative to the 400-ppm baseline. That is, the downwelling solar radiative energy flux was reduced by

$$\Delta S^\downarrow = -3.7 \text{ W}\cdot\text{m}^{-2} \log_2 \left(\frac{[\text{CO}_2]}{400 \text{ ppm}} \right), \quad [1]$$

and this offset was applied in both the subtropical LES domain and the tropical column.

In the tropical column of our modeling setup, the instantaneous radiative forcing at TOA when CO₂ concentrations are doubled from 400 to 800 ppm is $3.7 \text{ W}\cdot\text{m}^{-2}$; the adjusted radiative forcing after the stratosphere has equilibrated is $4.7 \text{ W}\cdot\text{m}^{-2}$. In the tropical column, the $3.7 \text{ W}\cdot\text{m}^{-2}$ reduction of the downwelling solar radiative energy flux, given our overall tropical albedo of 0.16, implies a $(1 - 0.16) \times 3.7 \text{ W}\cdot\text{m}^{-2} = 3.1 \text{ W}\cdot\text{m}^{-2}$ reduction of the net solar radiative-energy flux. This leaves uncompensated 34% ($1.6 \text{ W}\cdot\text{m}^{-2}$) of the adjusted CO₂ longwave radiative forcing. Similarly, in the subtropical LES domain, the adjusted TOA longwave radiative forcing for doubling CO₂ concentrations is $2.7 \text{ W}\cdot\text{m}^{-2}$, as determined by the regression method of Gregory et al. (32) after an abrupt CO₂ doubling from 400 to 800 ppm. The TOA albedo in the subtropical LES domain in the baseline simulation is 0.48, so a $3.7 \text{ W}\cdot\text{m}^{-2}$ reduction of the downwelling solar radiative energy flux implies a $(1 - 0.48) \times 3.7 \text{ W}\cdot\text{m}^{-2} = 1.9 \text{ W}\cdot\text{m}^{-2}$ reduction of the net solar radiative-energy flux. This leaves uncompensated 29% ($0.8 \text{ W}\cdot\text{m}^{-2}$) of the CO₂ longwave radiative forcing in the subtropical LES domain. This uncompensated forcing contributes to the warming we see in the simulations. However, in the subtropical LES domain, it is dwarfed by the change in shortwave CRE caused by the thinning of the subtropical clouds (Fig. 2C): CRE decreases by $7.8 \text{ W}\cdot\text{m}^{-2}$ from the steady state of the 400-ppm simulation to that of the 800-ppm simulation. Evidence that the direct CO₂ effect on cloud cover predominates in the cloud thinning as CO₂ concentrations increase comes from comparison of the simulations with and without solar geoengineering: The LWP reductions in the simulations with solar geoengineering (with or without subsidence weakening) are generally similar (within about 15%) to those in the corresponding simulations without solar geoengineering (27), although the surface warming in the simulations with solar geoengineering is muted by about a factor of 2.

For simulations with CO₂ concentrations below 400 ppm, we left the insolation fixed because plausible mechanisms for solar geoengineering to prevent climate cooling have not been proposed.

Simulations. We performed three sets of simulations, with three different choices for the subsidence velocity that advects the LES's native specific entropy and total water-specific humidity, thus providing entropy and moisture sources/sinks from unresolved large-scale dynamics. In the first set, the

subsidence velocity was fixed. One series of simulations in this set takes as its initial condition a snapshot of the 400-ppm baseline simulation after it has reached a statistically steady state. CO₂ concentrations then were increased in steps, and TOA insolation was reduced commensurately, up to a CO₂ concentration of 2,400 ppm. Another series of simulations was started from the 2,400-ppm run (from a snapshot 200 d into the simulation); CO₂ concentrations were then decreased again, and TOA insolation was commensurately increased until a CO₂ concentration of 400 ppm was reached. At CO₂ concentrations below 400 ppm (i.e., 200 and 300 ppm), no modification of the TOA insolation was made relative to the baseline.

The second and third set of simulations followed the same protocol as the first set with increasing CO₂ concentrations, but weakening large-scale subsidence in response to changes of the tropical SST, as described in ref. 27. The assumption that large-scale subsidence in the troposphere weakens under warming is based on theoretical arguments and climate simulations showing such weakening in global warming scenarios without solar geoengineering (34, 36, 51). We chose the same parameterization of subsidence

weakening for consistency with our previous study (27), without it being clear how realistic this subsidence weakening is in the presence of solar geoengineering.

Data Availability. All data needed to evaluate the conclusions in the paper are present in the paper. The source code for the simulations is available at climate-dynamics.org/software/#pycles.

ACKNOWLEDGMENTS. We thank Clare Singer for assistance with data processing. This research was made possible by the generosity of Eric and Wendy Schmidt by recommendation of the Schmidt Futures program, by Earthrise Alliance, Mountain Philanthropies, the Paul G. Allen Family Foundation, Charles Trimble, and NSF Grant AGS-1835860. The computations were performed on the California Institute of Technology's (Caltech's) High Performance Cluster, which is partially supported by a grant from the Gordon and Betty Moore Foundation. Part of this research was carried out at the Jet Propulsion Laboratory, Caltech, under a contract with NASA. C.M.K. and K.G.P. were at Caltech while carrying out this research.

1. K. Caldeira, L. Wood, Global and Arctic climate engineering: Numerical model studies. *Phil. Trans. R. Soc. Lond. A* **366**, 4039–4056 (2008).
2. G. Bala, Problems with geoengineering schemes to combat climate change. *Curr. Science* **96**, 41–48 (2009).
3. B. Kravitz *et al.*, Climate model response from the geoengineering model intercomparison project (GeoMIP). *J. Geophys. Res. Atmos.* **118**, 8320–8332 (2013).
4. G. Pitari *et al.*, Stratospheric ozone response to sulfate geoengineering: Results from the geoengineering model intercomparison project (GeoMIP). *J. Geophys. Res. Atmos.* **119**, 2629–2653 (2014).
5. S. Tilmes *et al.*, CESM1 (WACCM) stratospheric aerosol geoengineering large ensemble project. *Bull. Amer. Meteor. Soc.* **99**, 2361–2371 (2018).
6. J. B. Moreno-Cruz, K. L. Ricke, D. W. Keith, A simple model to account for regional inequalities in the effectiveness of solar radiation management. *Climatic Change* **110**, 649–668 (2012).
7. B. Kravitz *et al.*, A multi-model assessment of regional climate disparities caused by solar geoengineering. *Env. Res. Lett.* **9**, 074013 (2014).
8. H. Muri *et al.*, Climate response to aerosol geoengineering: A multimethod comparison. *J. Climate* **31**, 6319–6340 (2018).
9. G. Bala, P. B. Duffy, K. E. Taylor, Impact of geoengineering schemes on the global hydrological cycle. *Proc. Natl. Acad. Sci.* **105**:7664–7669 (2008).
10. K. Caldeira, G. Bala, L. Cao, The science of geoengineering. *Ann. Rev. Earth Planet. Sci.* **41**, 231–256 (2013).
11. H. D. Matthews, L. Cao, K. Caldeira, Sensitivity of ocean acidification to geoengineered climate stabilization. *Geophys. Res. Lett.* **36**, L10706 (2009).
12. National Research Council, *Climate Intervention: Reflecting Sunlight to Cool Earth* (The National Academies Press, Washington, DC, 2015).
13. A. Jones *et al.*, The impact of abrupt suspension of solar radiation management (termination effect) in experiment G2 of the Geoengineering Model Intercomparison Project (GeoMIP). *J. Geophys. Res. Atmos.* **118**, 9743–9752 (2013).
14. M. G. Lawrence *et al.*, Evaluating climate geoengineering proposals in the context of the Paris Agreement temperature goals. *Nature Comm.* **9**, 3734 (2018).
15. C. H. Trisos *et al.*, Potentially dangerous consequences for biodiversity of solar geoengineering implementation and termination. *Nature Ecol. Evol.* **2**, 475–482 (2018).
16. J. Gregory, M. Webb, Tropospheric adjustment induces a cloud component in CO₂ forcing. *J. Climate* **21**, 58–71 (2008).
17. T. Andrews, P. M. Forster, CO₂ forcing induces semi-direct effects with consequences for climate feedback interpretations. *Geophys. Res. Lett.* **35**, L04802 (2008).
18. M. C. Wyant, C. S. Bretherton, P. N. Blossey, M. Khairoutdinov, Fast cloud adjustment to increasing CO₂ in a superparameterized climate model. *J. Adv. Model. Earth Sys.* **4**, M05001 (2012).
19. M. D. Zelinka *et al.*, Contributions of different cloud types to feedbacks and rapid adjustments in CMIP5. *J. Climate* **26**, 5007–5027 (2013).
20. D. M. Roms, Climate sensitivity and the direct effect of carbon dioxide in a limited-area cloud-resolving model. *J. Climate* **33**, 3413–3429 (2020).
21. C. S. Bretherton, M. C. Wyant, Moisture transport, lower-tropospheric stability, and decoupling of cloud-topped boundary layers. *J. Atmos. Sci.* **54**, 148–167 (1997).
22. R. Wood, Stratocumulus clouds. *Mon. Wea. Rev.* **140**, 2373–2423 (2012).
23. C. S. Bretherton, P. N. Blossey, C. R. Jones, Mechanisms of marine low cloud sensitivity to idealized climate perturbations: A single-LES exploration extending the CGILS cases. *J. Adv. Model. Earth Sys.* **5**, 316–337 (2013).
24. C. S. Bretherton, Insights into low-latitude cloud feedbacks from high-resolution models. *Phil. Trans. R. Soc. Lond. A* **373**, 20140415 (2015).
25. P. N. Blossey *et al.*, CGILS Phase 2 LES intercomparison of response of subtropical marine low cloud regimes to CO₂ quadrupling and a CMIP3 composite forcing change. *J. Adv. Model. Earth Sys.* **8**, 1714–1726 (2016).
26. Z. Tan, T. Schneider, J. Teixeira, K. G. Pressel, Large-eddy simulation of subtropical cloud-topped boundary layers: 2. Cloud response to climate change. *J. Adv. Model. Earth Sys.* **9**, 19–38 (2017).
27. T. Schneider, C. M. Kaul, K. G. Pressel, Possible climate transitions from breakup of stratocumulus decks under greenhouse warming. *Nature Geosci.* **12**, 163–167 (2019).
28. M. Zhang *et al.*, CGILS: Results from the first phase of an international project to understand the physical mechanisms of low cloud feedbacks in general circulation models. *J. Adv. Model. Earth Sys.* **5**, 826–842 (2013).
29. Z. Tan, T. Schneider, J. Teixeira, K. G. Pressel, Large-eddy simulation of subtropical cloud-topped boundary layers: 1. A forcing framework with closed surface energy balance. *J. Adv. Model. Earth Sys.* **8**, 1565–1585 (2016).
30. R. T. Pierrehumbert, Thermostats, radiator fins, and the local runaway greenhouse. *J. Atmos. Sci.* **52**, 1784–1806 (1995).
31. P. M. Forster, P. G. Timothy Andrews, J. M. Gregory, L. S. Jackson, M. Zelinka, Evaluating adjusted forcing and model spread for historical and future scenarios in the CMIP5 generation of climate models. *J. Geophys. Res.* **118**, 1139–1150 (2013).
32. J. M. Gregory *et al.*, A new method for diagnosing radiative forcing and climate sensitivity. *Geophys. Res. Lett.* **31**, L03205 (2004).
33. A. K. Betts, Climate-convection feedbacks: Some further issues. *Climatic Change* **39**, 35–38 (1998).
34. I. M. Held, B. J. Soden, Robust responses of the hydrological cycle to global warming. *J. Climate* **19**, 5686–5699 (2006).
35. G. A. Vecchi *et al.*, Weakening of tropical Pacific atmospheric circulation due to anthropogenic forcing. *Nature* **441**, 73–76 (2006).
36. T. Schneider, P. A. O'Gorman, X. J. Levine, Water vapor and the dynamics of climate changes. *Rev. Geophys.* **48**, RG3001 (2010).
37. T. M. Merlis, Direct weakening of tropical circulations from masked CO₂ radiative forcing. *Proc. Natl. Acad. Sci.* **112**, 13167–13171 (2015).
38. B. A. Albrecht, C. S. Bretherton, D. Johnson, W. H. Schubert, A. S. Frisch, The Atlantic stratocumulus transition experiment—ASTEX. *Bull. Amer. Meteor. Soc.* **76**, 889–904 (1995).
39. I. Sandu, B. Stevens, R. Pincus, On the transitions in marine boundary layer cloudiness. *Atmos. Chem. Phys.* **10**, 2377–2391 (2010).
40. I. Sandu, B. Stevens, On the factors modulating the stratocumulus to cumulus transitions. *J. Atmos. Sci.* **68**, 1865–1881 (2011).
41. D. Chung, G. Matheou, J. Teixeira, Steady-state large-eddy simulations to study the stratocumulus to shallow cumulus cloud transition. *J. Atmos. Sci.* **69**, 3264–3276 (2012).
42. M. Meinshausen *et al.*, The RCP greenhouse gas concentrations and their extensions from 1765 to 2300. *Climatic Change* **109**, 213–241 (2011).
43. T. Schneider *et al.*, Climate goals and computing the future of clouds. *Nat. Clim. Change* **7**, 3–5 (2017).
44. K. G. Pressel, C. M. Kaul, T. Schneider, Z. Tan, S. Mishra, Large-eddy simulation in an anelastic framework with closed water and entropy balances. *J. Adv. Model. Earth Sys.* **7**, 1425–1456 (2015).
45. G. S. Jiang, C. W. Shu, Efficient implementation of weighted ENO schemes. *J. Comp. Phys.* **126**, 202–228 (1996).
46. A. H. Sobel, J. Nilsson, L. M. Polvani, The weak temperature gradient approximation and balanced tropical moisture waves. *J. Atmos. Sci.* **58**, 3650–3665 (2001).
47. R. Eastman, S. G. Warren, C. J. Hahn, Variations in cloud cover and cloud types over the ocean from surface observations, 1954–2008. *J. Climate* **24**, 5914–5934 (2011).
48. M. J. Iacono *et al.*, Radiative forcing by long-lived greenhouse gases: Calculations with the AER radiative transfer models. *J. Geophys. Res.* **113**, D13103 (2008).
49. T. W. Cronin, On the choice of average solar zenith angle. *J. Atmos. Sci.* **71**, 2994–3003 (2014).
50. H. W. Barker, J. N. S. Cole, J. Li, B. Yi, P. Yang, Estimation of errors in two-stream approximations of the solar radiative transfer equation for cloudy-sky conditions. *J. Atmos. Sci.* **72**, 4053–4074 (2015).
51. G. A. Vecchi, B. J. Soden, Global warming and the weakening of the tropical circulation. *J. Climate* **20**, 4316–4340 (2007).